International Journal of Heat and Mass Transfer 220 (2024) 124946

Contents lists available at ScienceDirect

International Journal of Heat and Mass Transfer

journal homepage: www.elsevier.com/locate/ijhmt

Thermal spreading resistance from an isothermal source into a finite-thickness body

Ankur Jain

Mechanical and Aerospace Engineering Department, University of Texas at Arlington, 500 W First St, Rm 211, Arlington, TX 76019, United States

ARTICLE INFO

Keywords:
Thermal spreading resistance
Thermal constriction resistance
Heat sink design
Thermal spreader design
Microelectronics thermal management

ABSTRACT

Thermal spreading resistance is encountered during two-dimensional thermal conduction from a hot surface into a body. Thermal spreading and the opposite problem of thermal constriction resistance are of much technological relevance in the design of heat sinks and thermal spreaders for thermal management of microelectronics and other heat-generating devices. Much of the past work in the theoretical analysis of thermal spreading is based on a source with given heat flux. In contrast, the isothermal source problem presents difficulties due to the resulting mixed nature of the boundary condition, due to which, only approximate solutions are available. This work derives the steady-state thermal spreading resistance from an isothermal source into a finite-thickness slab or cylinder. The mixed boundary condition is handled by posing it in the form of a spatially varying convective boundary condition, with a sufficiently large Biot number over the source to represent its isothermal nature. A series solution for the problem is derived, along a sufficient set of linear algebraic equations to determine the series coefficients. Results are shown to agree well with finite-element simulations. Results are compared with previously-reported approximate solutions within the parametric range of validity of the approximate solutions. The impact of key non-dimensional parameters on thermal spreading resistance is quantified. It is shown that thermal spreading resistance increases with decreasing size of the isothermal heat source, as expected. A third-order polynomial correlation with very good accuracy is proposed. This work advances the theoretical understanding of a problem for which only approximate solutions have been reported in the past. Results presented here offer a practical tool for thermal design and optimization of a variety of practical thermal management problems involving spreading or constriction.

1. Introduction

Thermal spreading resistance occurs in thermal conduction processes when heat from a finite source enters a material of larger size [1,2]. Examples include thermal conduction from a semiconductor chip into the chip packaging [3] and thermal conduction from a hot body into a heat spreader [4]. Conversely, thermal constriction resistance occurs in the opposite problem, for example, in the transfer of heat from a large, hot body into a heat sink placed on its outer surface [5] and across bolted joints [6]. Thermal spreading and constriction play an important role in thermal management of microelectronics, both at the device [7] and package [3,8] scale, power electronics [9], LEDs [10] and heat sinks [5]. Spreading and constriction resistance is also encountered in other engineering fields involving potential fields, such as semiconductors [11, 12] and electromagnetics [13].

Spreading and constriction are opposite problems, and, therefore, can both be analyzed within a single mathematical framework [1,2]. Due to their technological importance, the literature on analysis of thermal spreading/constriction resistance spans several decades, starting from early papers [14,15] to more recent ones as summarized in several review articles and book chapters [1,2]. Thermal spreading has been studied in the context of three key geometries – a semi-infinite half-space [17], a flux channel [18], and a finite disk/plate [4]. Schematics of a finite Cartesian plate with a strip source and a finite cylindrical disk with a circular source are shown in Fig. 1(a) and 1(b), respectively. In both cases, the source is placed symmetrically on the top surface of the body. In this scenario, thermal spreading resistance occurs due to the two-dimensional nature of the temperature field as heat conducts and spreads from the hot source into the larger-sized body towards the sink plane [2]. Determining such spreading resistance and its dependence on problem parameters is critical for the thermal design of such systems.

In a finite geometry, thermal spreading resistance is defined as the difference between the total thermal resistance and the one-dimensional thermal resistance present in an equivalent one-dimensional problem

E-mail address: jaina@uta.edu.

https://doi.org/10.1016/j.ijheatmasstransfer.2023.124946
Received 4 April 2023; Received in revised form 6 November 2023; Accepted 7 November 2023
Available online 25 November 2023

Nomenclature

a	Half-width or radius of the hot source (m)
$\bar{a}$	Non-dimensional half-width or radius of the hot source
A	Half-width or radius of the body (m)
Bi_{sink}	Biot number at the sink plane
h_{sink}	Convective heat transfer coefficient at the sink plane ($Wm^{-2}K^{-1}$)
k	Thermal conductivity ($Wm^{-1}K^{-1}$)
L	Slab length (m)
q	Heat flow rate (W)
r	Coordinate in the radial direction (m)
R_{sp}	Thermal spreading resistance (KW^{-1})
t	Thickness of the body (m)
$\bar{t}$	Non-dimensional thickness of the body
T	Temperature (K)
T_∞	Ambient temperature (K)
T_0	Source temperature (K)
T	Temperature (K)
x	Coordinate in the lateral direction (m)
z	Coordinate in the thickness direction (m)
ξ	Non-dimensional coordinate in the lateral/radial direction
η	Non-dimensional coordinate in the thickness direction
θ	Non-dimensional temperature

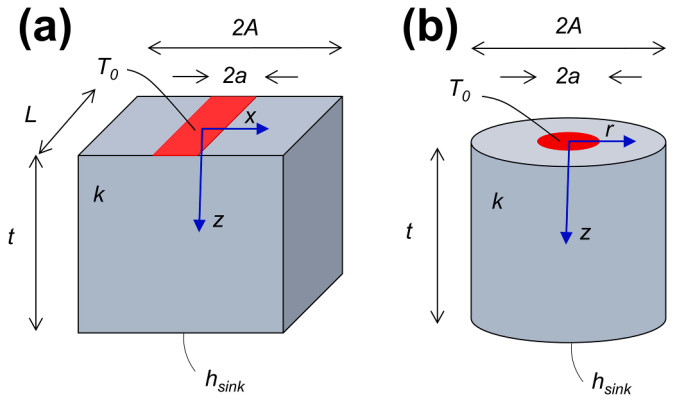

Fig. 1. Schematic of the geometry of a finite-thickness (a) slab, and (b) cylinder with uniform isothermal source and convective sink. In both cases, the source is located symmetrically on the top surface.

[2], and is based on either the maximum or average source temperature. In most cases involving the flux channel or finite disk/plate, the sidewalls are assumed to be adiabatic, although the analysis of edge cooling has gained recent interest [19]. The other end of the geometry away from the hot source, often referred to as the sink plane, is usually modeled as either isothermal, or with a convective heat transfer coefficient. A key geometrical parameter in these problems that determines the thermal spreading resistance is the size of the hot source and thickness of the slab/cylinder, both of which are usually non-dimensionalized by the edge length or radius of the slab/cylinder. Additionally, the convective heat transfer coefficient at the sink plane, often expressed in the form of a Biot number, is also an important parameter. In addition to the symmetric, single-layer geometry depicted in Fig. 1(a) and 1(b), analysis of multilayer geometry [20] and eccentrically-placed heat sources [21] has also been carried out. Orthotropic thermal conduction [16], inter-layer thermal contact resistance [22] and spatially-varying convective heat transfer coefficient at the sink plane [20] have also been accounted for.

In most of the past literature, the hot source is modeled as an isoflux surface [1,2]. This assumption aligns well with conditions in several applications such as microelectronic devices [3,8]. This scenario is also convenient to model, since the rest of the source plane is adiabatic, and, therefore, a spatially varying heat flux boundary condition – non-zero on the source surface and zero elsewhere – can be implemented. In contrast, the treatment of an isothermal source is also important because when the contact between non-smooth bodies occurs over an area smaller than the apparent area of contact due to surface roughness, the thermal condition along such an area of contact has been shown to be isothermal [23,24]. Therefore, the analysis of spreading resistance problem for an isothermal source is important for the study of interfacial heat transfer. Unfortunately, an isothermal source results in a mixed boundary condition at the source plane that is more difficult to mathematically model. At best, an isothermal source has been modeled approximately using a variable heat flux distribution that varies spatially as $\frac{1}{\sqrt{a^2-x^2}}$, where a is the source width and x is the coordinate along the source. This is known to result in a nearly isothermal temperature distribution at the source [2, 15]. Based on this, approximate expressions for the spreading resistance have been derived for a number of scenarios such as [2,15]. Such solutions are limited to small source width relative to the width of the body. An isothermal source problem has been solved using the method of conformal mapping, but only for a semi-infinite geometry [24]. A few highly mathematical treatments of the mixed problem are also available [25,26,27], which are difficult to apply directly to problems of practical relevance.

Despite such work, there remains an active interest in determining the thermal spreading resistance for an isothermal source without the approximation entailed in the variable heat flux approach in past literature. Doing so may result in models that are not limited in the manner that approximate isothermal models are, and may improve the accuracy of thermal resistance models.

This work presents theoretical analysis of thermal spreading from an isothermal source into a larger, finite-sized body. Both slab and cylinder geometries are considered. In each case, the mixed isothermal-adiabatic boundary condition is represented by a spatially-varying convective boundary condition, with a sufficiently large convective heat transfer coefficient over the source. A series solution for the temperature field is written, and coefficients for the series are determined by deriving a sufficient number of linear algebraic equations based on the spatially varying source convective heat transfer coefficient. Results are found to agree well with finite-element simulations, and are compared with previously-reported approximate solutions for this problem. Polynomial correlations with very small error are proposed for use in thermal design and optimization without the need for detailed mathematical analysis.

2. Problem definition

Consider the steady state problem of thermal spreading from a hot isothermal source into a larger but finite geometry. Two specific problems pertaining to a finite Cartesian slab and a cylindrical disk, each of thickness t and uniform, isotropic thermal conductivity k are considered, as depicted in Fig. 1(a) and 1(b), respectively. The half-width or radius of the slab/cylinder is denoted by A. In the case of the slab, a finite strip of half-width a and the same length L as the slab is assumed, whereas in the cylinder problem, a hot source of radius a is assumed to be located about the same axis as the cylinder, as shown in Fig. 1(a) and 1(b), respectively. In both cases, the hot source is located symmetrically around the center of the top surface, so that thermal conduction is two-

dimensional and, in the case of the slab, only one half of the body may be analyzed based on symmetry. Temperatures of the hot source and the ambient are denoted by T_0 and T_∞, respectively, where $T_0 > T_\infty$ in the thermal spreading problem. The region around the source on the top plane as well as the sidewalls are taken to be adiabatic, as is the usual case in the literature [1,2]. A general convective heat transfer boundary condition, characterized by a convective heat transfer coefficient h_{sink} and ambient temperature T_∞ is used to represent cooling along the sink plane located at $z = t$. The interest is in determining the temperature distribution $T(x,z)$ (slab) or $T(r,z)$ (cylinder) and thus calculate the thermal resistance defined as the ratio of temperature difference $(T_0 - T_\infty)$ and the total heat flow through the body. While this problem is defined here in the form of thermal spreading, the opposite problem of thermal constriction $(T_0 < T_\infty)$ can also be analyzed using the same framework.

3. Solution for a finite slab

The problem of thermal spreading resistance in the finite slab is considered first. Based on symmetry about the $x = 0$ plane, only the right half of the problem is considered. Since the source strip is as long as the body in the y direction, therefore, this is a two-dimensional problem, mathematically described as follows:

$$\frac{\partial^2 T}{\partial x^2} + \frac{\partial^2 T}{\partial z^2} = 0 \tag{1}$$

with the following boundary conditions:

$$\frac{\partial T}{\partial x} = 0 \quad (x = 0,\ A) \tag{2}$$

$$\begin{aligned} &T = T_0 \quad (0 < x < a) \\ &\frac{\partial T}{\partial z} = 0 \quad (a < x < A) \end{aligned} \qquad (z = 0) \tag{3}$$

$$-k\frac{\partial T}{\partial z} = h_{sink}(T - T_\infty) \quad (z = t) \tag{4}$$

This problem is non-dimensionalized as follows:

$$\theta = \frac{T - T_\infty}{T_0 - T_\infty};\ \xi = \frac{x}{A};\ \eta = \frac{z}{A};\ \bar{a} = \frac{a}{A};\ \bar{t} = \frac{t}{A};\ Bi_{sink} = \frac{h_{sink}A}{k} \tag{5}$$

which results in the following non-dimensional problem:

$$\frac{\partial^2 \theta}{\partial \xi^2} + \frac{\partial^2 \theta}{\partial \eta^2} = 0 \tag{6}$$

with the following boundary conditions:

$$\frac{\partial \theta}{\partial \xi} = 0 \quad (\xi = 0,\ 1) \tag{7}$$

$$\theta = 1 \quad (0 < \xi < \bar{a}) \frac{\partial \theta}{\partial \eta} = 0 (\bar{a} < \xi < 1)(\eta = 0) \tag{8}$$

$$-\frac{\partial \theta}{\partial \eta} = Bi_{sink} \cdot \theta \quad (\eta = \bar{t}) \tag{9}$$

The mixed boundary condition represented by Eq. (8) presents difficulties in solving this problem. For example, while the separation of variables method can easily solve a problem in which either a heat flux or a temperature distribution is specified over the entire $\eta = 0$ surface, it is much more difficult when temperature is specified over one region of the surface and heat flux over the rest. This difficulty has been addressed in the past through an approximate technique [2,15], in which, a specific heat flux distribution proportional to $\frac{1}{\sqrt{\bar{a}^2 - \xi^2}}$ known to produce a nearly isothermal surface is specified over $0 < \xi < \bar{a}$ instead of an isothermal condition. However, the solution so derived is approximate and valid only when $\bar{a}$ is very small. Instead of such an approximation, in the present work, the mixed boundary condition at $\eta = 0$ is expressed as a convective boundary condition over the entire surface using a Biot number $Bi(\xi)$ as follows:

$$\frac{\partial \theta}{\partial \eta} = Bi(\xi) \cdot (\theta - 1) \quad (\eta = 0) \tag{10}$$

where $Bi(\xi)$ is defined as

$$Bi(\xi) = Bi_{max} \cdot (1 - \mathscr{H}(\xi - \bar{a}))(\eta = 0) \tag{11}$$

Where $\mathscr{H}$ is the Heaviside function. Eq. (11) implies that $Bi = Bi_{max}$ for $0 < \xi < \bar{a}$ and zero for $\bar{a} < \xi < 1$. Choosing Bi_{max} to be sufficiently large results in constant temperature over the source $(0 < \xi < \bar{a})$, as desired, whereas the zero value of $Bi(\xi)$ defined over $\bar{a} < \xi < 1$ imposes an adiabatic condition in the rest of the source plane. In this manner, a single convective boundary condition with a spatially varying Biot number captures both aspects of the mixed boundary condition – the isothermal source and the adiabatic region around the source.

A solution for this problem is derived next using the separation of variables technique. First, a general solution is written in the following series form

$$\theta(\xi, \eta) = f_0(\eta) + \sum_{n=1}^{\infty} \cos(\lambda_n \xi) f_n(\eta) \tag{12}$$

where, based on the lateral boundary conditions given by Eq. (7), the sine term has been dropped, and further, the eigenvalues are $\lambda_n = n\pi$ $(n = 1, 2..\infty)$. Note that $f_0(\eta)$ corresponds to the $n = 0$ term, which must be considered separately due to adiabatic boundary conditions at both ends along the η direction [28].

Inserting Eq. (12) in the governing energy equation, one may show that

$$f_0(\eta) = C_0\eta + D_0 \tag{13}$$

and

$$f_n(\eta) = C_n \cosh(\lambda_n \eta) + D_n \sinh(\lambda_n \eta) \quad (n = 1, 2..\infty) \tag{14}$$

The boundary condition at the sink plane is used next, based on which, one may derive $D_0 = p_0 C_0$ and $D_n = p_n C_n$, where $p_0 = -\left(\bar{t} + \frac{1}{Bi_{sink}}\right)$ and

$$p_n = -Bi_{sink} \cosh \frac{(\lambda_n \bar{t}) + \lambda_n \sinh(\lambda_n \bar{t})}{Bi_{sink} \sinh(\lambda_n \bar{t}) + \lambda_n \cosh(\lambda_n \bar{t})} (n = 1, 2..\infty) \tag{15}$$

Therefore, the temperature field may be written in the following form:

$$\theta(\xi, \eta) = C_0[\eta + p_0] + \sum_{n=1}^{\infty} C_n \cos(\lambda_n \xi)[\cosh(\lambda_n \eta) + p_n \sinh(\lambda_n \eta)] \tag{16}$$

Note that the first term in the solution corresponds to the solution of the one-dimensional thermal conduction problem without thermal spreading if the source were as wide as the body.

In order to determine the remaining coefficients C_0 and C_n that appear in the solution, the convective boundary condition at the source plane with spatially varying Biot number, given by Eq. (10) is used. Inserting Eq. (16) in Eq. (10) results in

$$C_0 + \sum_{n=1}^{N} \lambda_n C_n p_n \cos(\lambda_n \xi) = Bi(\xi) \left[p_0 C_0 - 1 + \sum_{n=1}^{N} C_n \cos(\lambda_n \xi) \right] \tag{17}$$

where, for practical computation, the infinite series has been truncated to a sufficiently large value of N. A total of $(N+1)$ linear algebraic equations are then derived in order to determine the $(N+1)$ unknowns C_0 and C_n $(n = 1, 2..N)$ as follows: First, Eq. (17) is integrated from $\xi = 0$

to $\xi = 1$. For the form of $Bi(\xi)$ given by Eq. (11), this results in

$$C_0\left[\frac{1}{Bi_{max}} - p_0\bar{a}\right] - \sum_{n=1}^{N} C_n \frac{\sin(\lambda_n \bar{a})}{\lambda_n} = -\bar{a} \tag{18}$$

Further, Eq. (17) is multiplied by $\cos(\lambda_m \xi)$ $(m = 1, 2 \ldots N)$ and then, in each case, integrated from $\xi = 0$ to $\xi = 1$, leading to

$$-p_0 C_0 \frac{\sin(\lambda_m \bar{a})}{\lambda_m} + C_m\left[\frac{\lambda_m p_m}{2Bi_{max}} - \frac{\bar{a}}{2} - \frac{\sin(2\lambda_m \bar{a})}{4\lambda_m}\right] - \sum_{n=1\ n\neq m}^{N} C_n \lambda_n \sin(\lambda_n \bar{a})\cos(\lambda_m \bar{a}) - \lambda_m \cos\frac{(\lambda_n \bar{a})\sin(\lambda_m \bar{a})}{\lambda_n^2 - \lambda_m^2} = -\frac{\sin(\lambda_m \bar{a})}{\lambda_m} \tag{19}$$

Eq. (18) and Eq. (19) for $m = 1, 2 \ldots N$ constitute a total of $N + 1$ equations in $N + 1$ unknowns, which can be easily solved to determine C_0 and C_n, and hence complete the derivation of the solution.

Note that the technique used above to determine a sufficient set of linear algebraic equations has been used in the past to solve other problems with spatially varying convective heat transfer coefficient [29–31]. This approach may be interpreted as a generalization of the usual procedure of determining coefficients for a constant Biot number problem using the principle of orthogonality. In such a case, several integrals obtained during the procedure outlined above become zero due to the constant Biot number coupled with integral properties of the eigenfunctions. This results in explicit expressions for the coefficients instead of a set of coupled algebraic equations in the present case of variable Biot number. Further note that truncating the infinite series to a finite number of terms is no worse than any practical computation of an infinite series, in which, only a finite number of terms are computed as well, similar to the present work. As shown later, the error can be reduced to an acceptable threshold by choosing a sufficiently large value of N.

The isothermal source is modeled here in the form of a convective boundary condition with a sufficiently large Bi_{max}. As a result, in order to ensure accuracy, Bi_{max} must be chosen to be a large number. In this case, $Bi_{max} = 1000$ is found to be sufficiently large, and further increase is not found to change the results significantly.

Considering only one half of the geometry shown in Fig. 1(a), heat flow through the slab, based on the temperature solution is

$$q = -k\int_0^a \left(\frac{\partial T}{\partial z}\right)_{z=0} L dx = -kL(T_0 - T_\infty)\left[C_0\bar{a} + \sum_{n=1}^{N} C_n p_n \sin(\lambda_n \bar{a})\right] \tag{20}$$

Note that while there is a singularity in the heat flux profile along the source plane due to the isothermal and adiabatic surfaces next to each other, this does not influence the derivation of the heat flux, since the integral in Eq. (20) above only goes up to $x = a$, within which, the heat flux is continuous.

Finally, the thermal spreading resistance is determined by computing the total thermal resistance and subtracting the 1D thermal resistance comprising conduction resistance through the body and boundary convective resistance. This results in the following expression for the non-dimensional thermal spreading resistance of half of the geometry shown in Fig. 1(a).

$$kLR_{sp} = -\left[C_0\bar{a} + \sum_{n=1}^{N} C_n p_n \sin(\lambda_n \bar{a})\right]^{-1} + p_0 \tag{21}$$

Eq. (21) shows that, as expected, the non-dimensional spreading resistance depends on $\bar{a}$, the source half-width, $\bar{t}$, the body thickness and Bi_{sink} that represents convective conditions at the sink plane. Note that the thermal spreading resistance from Eq. (21) pertains to one half of the geometry shown in Fig. 1(a) in which the thermal conduction problem is solved above. If considering the entire geometry, total heat flow through the body will be twice as given by Eq. (20), and therefore, the thermal spreading resistance will be half of that calculated from Eq. (21).

While the result derived here predicts the spreading resistance for any source width $\bar{a}$, it is instructive to examine Eq. (21) in limiting conditions as $\bar{a} \to 1$. In such a case, Eq. (18) shows that $C_0 = p_0^{-1}$ since $\sin(\lambda_n) = 0$. Further, from Eq. (19), $C_m = 0$ $(m = 1, 2 \ldots N)$. Substituting in Eq. (21), it is found that $kLR_{sp} \to 0$ as $\bar{a} \to 1$. This limiting result is expected because as the source size approaches that of the body itself, there is no longer any thermal spreading, the temperature field is purely one-dimensional, and, therefore, the spreading resistance becomes zero. Therefore, the result derived here correctly reduces to an expected result in a limiting case.

4. Solution for a finite cylinder

A similar problem for thermal spreading resistance in a finite cylinder is shown schematically in Fig. 1(b). The non-dimensional coordinate ξ for this problem is defined as $\xi = \frac{r}{A}$ instead of $\xi = \frac{x}{A}$ in the slab problem. Definitions for all other non-dimensional parameters remain the same. $\bar{a}$ represents the non-dimensional radius of the source instead of the half-width in the slab problem. Since the solution procedure for this problem is similar to the slab problem, only the final expressions for the temperature field and thermal spreading resistance are provided here for brevity. The non-dimensional temperature distribution, comprising Bessel functions of the first kind instead of cosine functions is given by

$$\theta(\xi, \eta) = \widehat{C}_0(\eta + p_0) + \sum_{n=1}^{\infty} \widehat{C}_n \mathrm{J}_0(\mu_n \xi)(\cosh(\mu_n \eta) + p_n \sinh(\mu_n \eta)) \tag{22}$$

Where J_0 is the zeroth-order Bessel function of the first kind [32], and μ_n are roots of J_1, the first-order Bessel function of the first kind. Note that, similar to the slab problem, the series solution may be truncated to a finite number of terms, N, for computational purposes, and the coefficients may be determined by solving the following set of algebraic equations

$$\widehat{C}_0\left[\frac{1}{2Bi_{max}} - p_0\frac{\bar{a}^2}{2}\right] - \sum_{n=1}^{N} \widehat{C}_n \frac{\bar{a}\mathrm{J}_1(\lambda_n \bar{a})}{\lambda_n} = -\frac{\bar{a}^2}{2} \tag{23}$$

$$-\widehat{C}_0 p_0 \frac{\bar{a}\mathrm{J}_1(\lambda_n \bar{a})}{\lambda_n} + \widehat{C}_m\left[\frac{\lambda_m p_m \mathrm{J}_0^2(\lambda_m)}{2Bi_{max}} - \frac{\bar{a}^2}{2}\left(\mathrm{J}_0^2(\lambda_m \bar{a}) + \mathrm{J}_1^2(\lambda_m \bar{a})\right)\right] - \sum_{n=1\ n\neq m}^{N} \widehat{C}_n \bar{a}\lambda_n \mathrm{J}_1(\lambda_n \bar{a})\mathrm{J}_0(\lambda_m \bar{a}) - \lambda_m \mathrm{J}_1 \frac{(\lambda_m \bar{a})\mathrm{J}_0(\lambda_n \bar{a})}{\lambda_n^2 - \lambda_m^2} = -\frac{\bar{a}\mathrm{J}_1(\lambda_m \bar{a})}{\lambda_m} \tag{24}$$

This may be shown to result in the following expression for the thermal spreading resistance for a finite-thickness cylinder:

$$2\pi kAR_{sp} = -\left[\widehat{C}_0\frac{\bar{a}^2}{2} + \bar{a}\sum_{n=1}^{N}\widehat{C}_n p_n \mathrm{J}_1(\lambda_n\bar{a})\right]^{-1} + 2p_0 \tag{25}$$

Similar to the discussion at the end of the previous Section, it can be shown here that as $\bar{a}\to 1$, the thermal spreading resistance approaches zero due to the one-dimensional nature of the temperature field in this limiting case.

5. Results and discussion

5.1. Convergence of the series solution

A fundamental premise of the theoretical technique used here is to represent the mixed isothermal-adiabatic boundary condition with a spatially varying convective boundary condition, and then to derive algebraic equations for the series coefficients. Therefore, it is important to determine how the number of terms considered affects the accuracy of the computed solution. In order to do so, a relative error $\delta(N) = \frac{|R_{sp}(N)-R_{sp,\infty}|}{R_{sp,\infty}} \times 100$ is defined as the % deviation between the thermal spreading resistance with a finite number of terms, N, compared to one computed with a very large number of terms, in this case, 200 terms. The convergence of δ with increasing N must be examined in order to determine the number of terms needed to obtain a desired level of accuracy.

For the slab problem, Fig. 2(a) plots δ as a function of N for two different values of the source strip width $\bar{a}$. Other problem parameters are $\bar{t} = 0.4$, $Bi_{sink} = 1000$. Fig. 2(a) indicates somewhat slow convergence of the series solution. For example, at $\bar{a} = 0.1$, more than 37 and 64 terms are needed for the computed thermal spreading resistance to be within 10% and 5%, respectively, of the value computed with a very large number of terms. Convergence analysis for the cylinder problem, shown in Fig. 2(b) for the same set of non-dimensional parameters, also shows similar characteristics, with 70 and 111 terms needed in order for the error to be within 10% and 5%, respectively, for $\bar{a} = 0.1$. In both problems, results for the two source widths shown are quite similar.

Note that slow convergence of the series solution is not necessarily a significant computational hindrance, since the eigenvalues for this problem are independent of all problem parameters and can be computed quite easily, given by roots of the cosine function and first-order Bessel function of the first kind for the slab and cylinder problems, respectively. Moreover, solving a set of linear equations is computationally inexpensive even when the number of equations is a few hundred. It is found in this work that the thermal spreading resistance can be calculated within less than 0.2 s even with 200 terms and no computational optimization.

Based on the results shown in Fig. 2, all subsequent analyses presented here are carried out with 200 terms.

5.2. Effect of Bi_{max}

Another key feature of the theoretical methodology used in this work is to represent the mixed boundary condition with a single convective boundary condition containing a spatially-varying Biot number. In order to satisfy the isothermal portion of the boundary condition over $0 < \xi < \bar{a}$, the Biot number is taken to be Bi_{max}, the value of which must be sufficiently large to force isothermal conditions in that region. Therefore, the value of Bi_{max} may impact the computed thermal spreading resistance, and it is important to determine how large Bi_{max} should be in order to accurately represent isothermal conditions. To investigate this, Fig. 3(a) presents a plot of the computed thermal spreading resistance at one particular set of parameters ($\bar{t} = 1.2$, $Bi_{sink} = 1000$) as a function of Bi_{max}. Curves are presented for three different values of $\bar{a}$. In addition, for $\bar{a} = 0.6$, Fig. 3(b) plots the computed temperature distribution along the source plane for four different values of Bi_{max}. Fig. 3 shows that for each thickness considered, the value of spreading resistance has significant error when Bi_{max} is relatively small, and converges beyond a value of around $Bi_{max} = 100$. Similarly, with $Bi_{max} = 100$, the computed temperature distribution is within a few % of the expected value of 1.0 in the isothermal region, with even greater accuracy at $Bi_{max} = 1000$. Therefore, a value of $Bi_{max} = 1000$ is used in this work in order to ensure that the isothermal conditions are being correctly satisfied.

5.3. Comparison with finite-element simulations

For verification of the theoretical model presented here, results are compared with finite-element simulations using a commercially available software. This comparison is presented in terms of temperature distribution along the thickness (η) and lateral (ξ) directions in Fig. 4(a) and 4(b), respectively. In each case, results are presented for both slab and cylinder problems. Other problem parameters are $\bar{a} = 0.1$, $\bar{t} = 0.4$ and $Bi_{sink} = 2.0$. For both slab and cylinder problems, Fig. 4 shows excellent agreement between the present work and finite-element simulations, in both thickness and lateral directions. In particular, the present work is found to correctly capture constant temperature

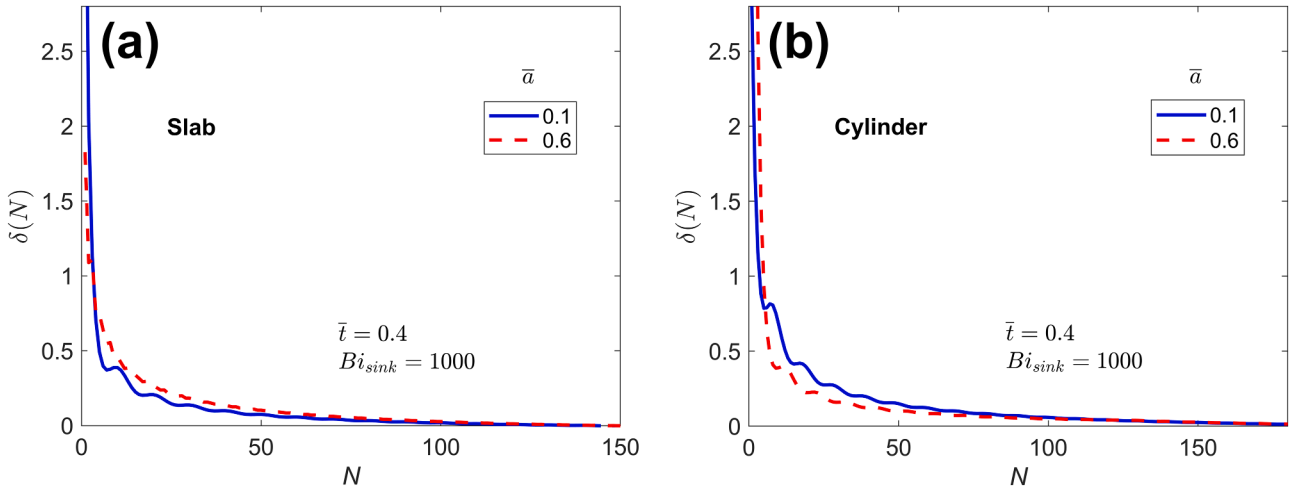

Fig. 2. Convergence of the series solution: Deviation of the computed thermal spreading resistance from the converged value as a function of number of terms for two different values of $\bar{a}$ for (a) slab, and (b) cylinder. Other parameters are $\bar{t} = 0.4$, $Bi_{sink} = 1000$.

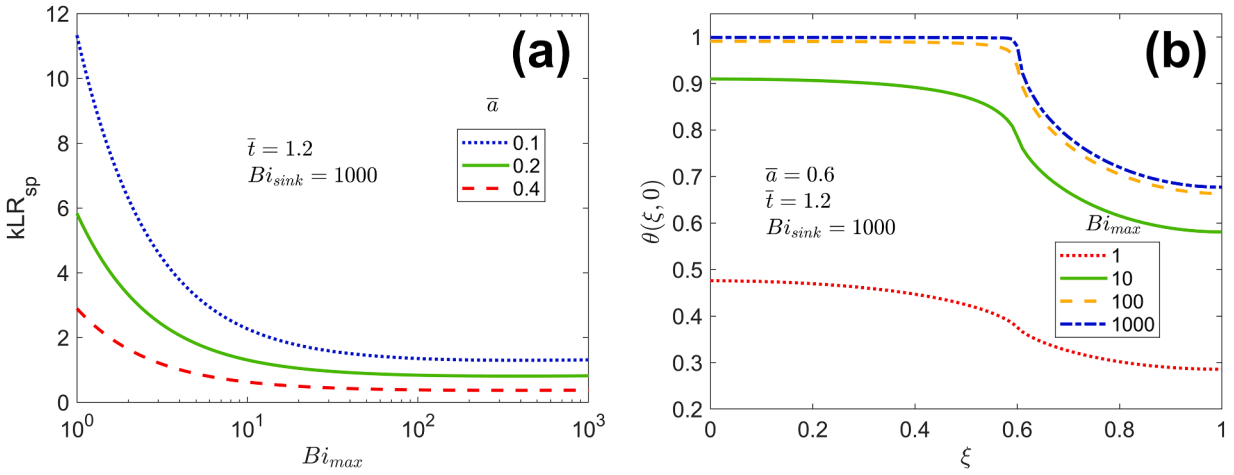

Fig. 3. Effect of Bi_{max}: (a) Thermal spreading resistance as a function of Bi_{max} for three different values of $\bar{a}$ and for $\bar{t} = 1.2$, $Bi_{sink} = 1000$. (b) Temperature distribution along the source plane for four different values of Bi_{max}. Other parameters are $\bar{a} = 0.6$, $\bar{t} = 1.2$, $Bi_{sink} = 1000$.

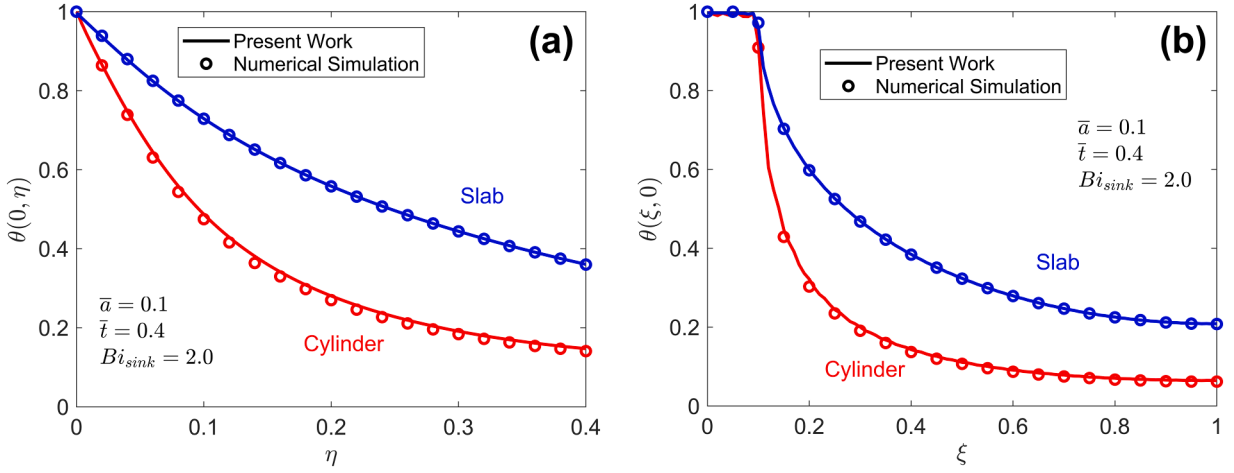

Fig. 4. Comparison of the present technique with finite-element simulations: (a) Temperature as a function of η at the center line ($\xi = 0$), (b) Temperature as a function of ξ at the source plane ($\eta = 0$). Results from the present work and a finite-element simulation are plotted for both slab and cylinder problems. Problem parameters are $\bar{a} = 0.1$, $\bar{t} = 0.4$, $Bi_{sink} = 2.0$.

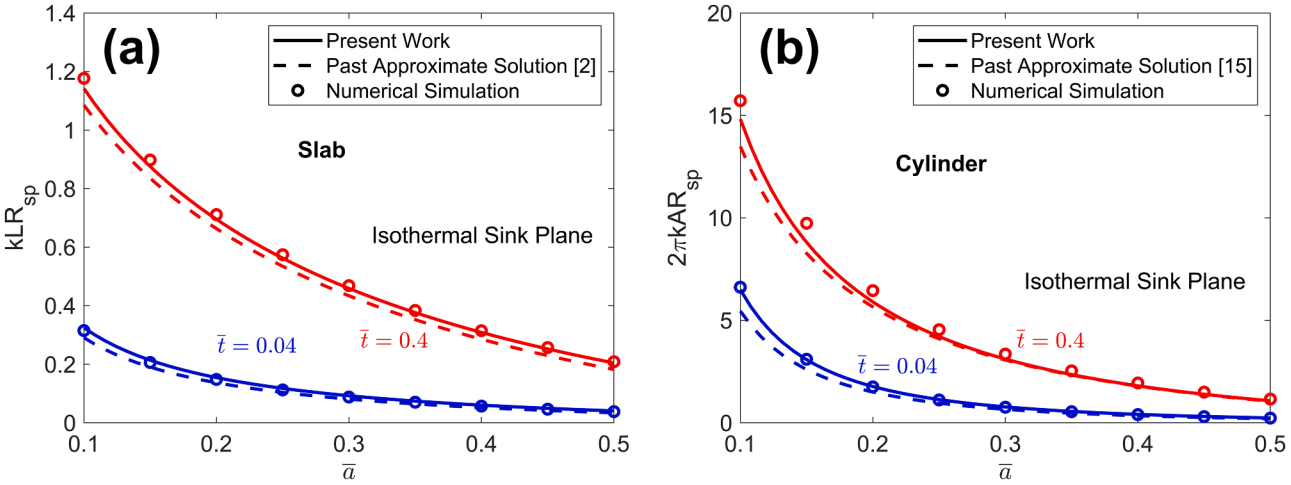

Fig. 5. Comparison of the present technique with past work: Spreading resistance as a function of source size $\bar{a}$ for two different values of $\bar{t}$: (a) Slab, (b) Cylinder. For comparison, results from past approximate solutions ([2] and [15], respectively) are also presented. The sink plane is taken to be isothermal for this comparison. Results from a numerical simulation are also shown.

condition along the lateral direction up to $\xi = \bar{a}$, corresponding to the isothermal source. The worst-case deviation between the present work and finite-element simulations is found to be less than 1%, which increases confidence in the theoretical derivation carried out here.

5.4. Comparison with past work

It is of interest to also compare results from the present work with approximate solutions available from past work. While most of the past literature on thermal spreading resistance modeling is based on an isoflux source, the case of an isothermal source has been addressed only in a limited number of papers. An exact solution is available only for a semi-infinite flux tube, which is an extreme case of the present work ($\bar{t}\to\infty$) [21]. For the finite geometry considered here, the problem of isothermal source and the subsequent mixed boundary condition has been solved approximately by representing the isothermal source with a spatially-varying heat flux proportional to $\frac{1}{\sqrt{\bar{a}^2-\xi^2}}$. It has been shown that such a heat flux produces an approximately isothermal distribution along the source [2,15]. Based on this, the following approximate expressions for the non-dimensional thermal spreading resistance have been derived:

For the slab problem [2],

$$kLR_{sp} = \frac{1}{\bar{a}\pi^2}\sum_{n=1}^{\infty}\frac{\sin(\lambda_n\bar{a})}{n^2}\mathrm{J}_0(\lambda_n\bar{a})\frac{\lambda_n + \mathrm{Bi}_{sink}\cdot\tanh(\lambda_n\bar{t})}{\lambda_n\cdot\tanh(\lambda_n\bar{t}) + \mathrm{Bi}_{sink}} \tag{26}$$

For the cylinder problem [15] with isothermal sink conditions,

$$2\pi kAR_{sp} = \frac{4}{\bar{a}^2}\sum_{n=1}^{\infty}\mathrm{J}_1\frac{(\mu_n\bar{a})\sin(\mu_n\bar{a})}{\mu_n^3\cdot\mathrm{J}_1(\mu_n)}\tan(\mu_n\bar{t}) \tag{27}$$

Comparison between results from the present work and the approximate results cited above is presented in Fig. 5(a) and 5(b) for the slab and cylinder problems, respectively. For reference, results from a numerical simulation are also presented. In each case, the non-dimensional thermal spreading resistance is plotted as a function of the source size $\bar{a}$. Plots are presented for two different values of the thickness $\bar{t}$. For both slab and cylinder geometries, Fig. 5 shows good agreement between the solution derived here and the approximate solution from past work based on heat flux approximation of the isothermal source. Both models predict similar trends, and the small difference between the two is likely due to the approximate nature of previously available results, Eqs. (26) and (27). There is good agreement, in general, with results from numerical simulations.

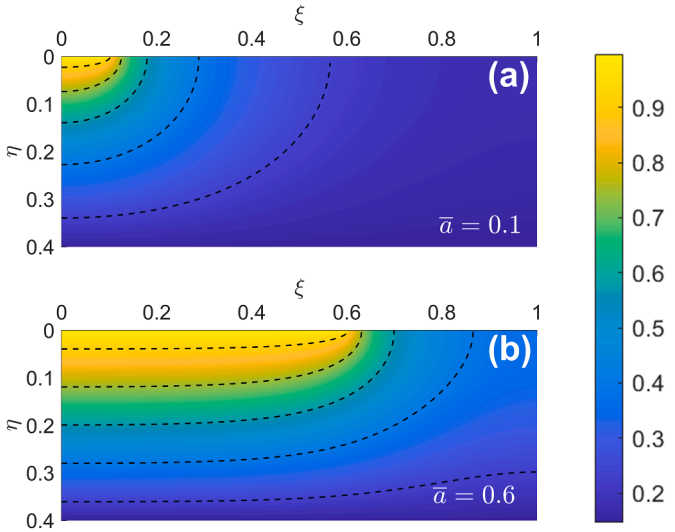

Fig. 6. Colorplots of computed temperature distribution in the finite slab for (a) $\bar{a} = 0.1$, (b) $\bar{a} = 0.6$. Other parameters are $\bar{t} = 0.4$, $Bi_{sink} = 1000$. Isotherms corresponding to $\theta = 0.9,\ 0.7,\ 0.5,\ 0,3,\ 0.1$ are also shown.

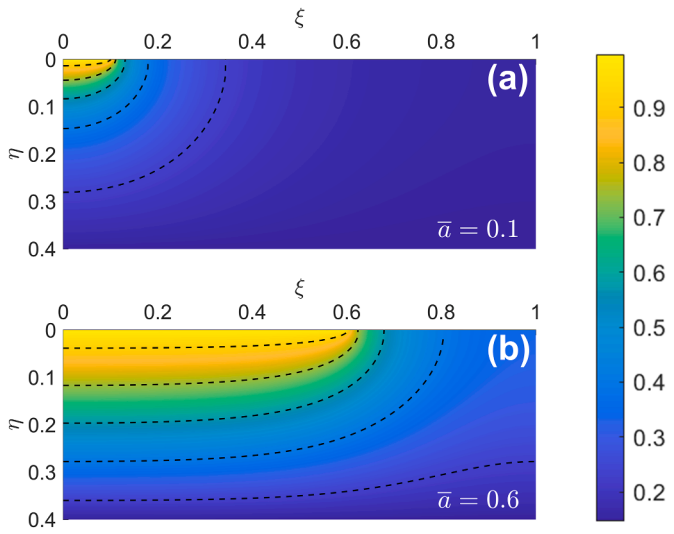

Fig. 7. Colorplots of computed temperature distribution in the finite cylindrical disk for (a) $\bar{a} = 0.1$, (b) $\bar{a} = 0.6$. Other parameters are $\bar{t} = 0.4$, $Bi_{sink} = 1000$. Isotherms corresponding to $\theta = 0.9,\ 0.7,\ 0.5,\ 0,3,\ 0.1$ (top to down) are also shown.

5.5. Typical temperature distribution colorplots

Based on the solution for the temperature distribution derived in Sections 3 and 4, colorplots of the temperature field are presented in Figs. 6 and 7 for the slab and cylinder problems, respectively. In each case, colorplots are presented for two cases – $\bar{a} = 0.1$ and $\bar{a} = 0.6$. Isotherm curves corresponding to $\theta = 0.9,\ 0.7,\ 0.5,\ 0.3$ and 0.1 are also plotted in order to illustrate the two-dimensional nature of heat flow.

In each case, as expected, temperature is highest at the source and gradually reduces with increasing ξ and/or η. The temperature distribution is found to be flat at both $\xi = 0$ and $\xi = 1$, consistent with adiabatic boundary conditions at the two ends. At the source plane, temperature is found to be very close to 1 up to $\xi = \bar{a}$ in each case, representative of the isothermal source. Isotherms close to the source are found to be curved in nature, indicating thermal spreading, and become flatter as one approaches the sink plane. Isotherm lines along the ξ di-

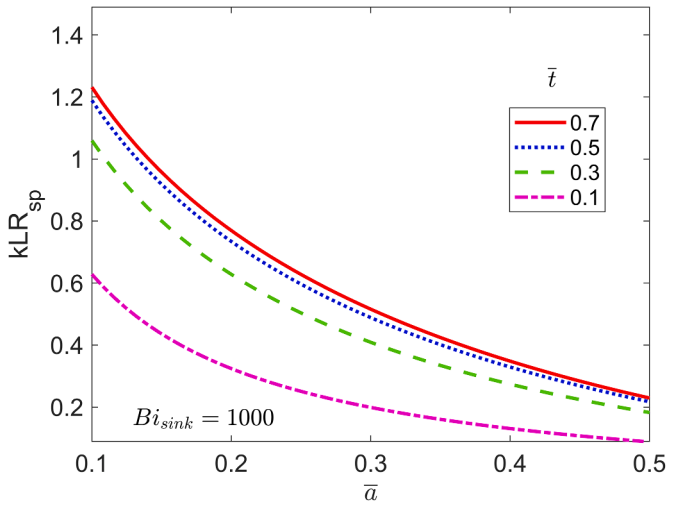

Fig. 8. Effect of source width on thermal spreading resistance: Spreading resistance as a function of source size $\bar{a}$ for multiple values of $\bar{t}$ with $Bi_{sink} = 1000$ for the slab problem.

rection are closer to each other for $\bar{a} = 0.1$ compared to $\bar{a} = 0.6$, which is indicative of greater thermal spreading in the lateral direction when the source is relatively small in size. This confirms that R_{sp} is larger for smaller values of $\bar{a}$. This is investigated in more detail in a subsequent sub-section.

5.6. Effect of non-dimensional parameters on spreading resistance

The non-dimensional thermal spreading resistance derived in this work depends on three key non-dimensional parameters - $\bar{a}$, the non-dimensional source half-width/radius, $\bar{t}$, the non-dimensional body thickness, and Bi_{sink}, the Biot number governing convective heat removal at the sink plane. It is instructive to further understand how the thermal spreading resistance depends on these parameters.

The dependence of thermal spreading resistance on $\bar{a}$ is examined first. Fig. 8 plots kLR_{sp} as a function of $\bar{a}$ for four different slab thicknesses. In each case, a large value of Bi_{sink}, consistent with isothermal conditions is assumed. It is found that in each case, the spreading resistance reduces as $\bar{a}$ increases. This is expected since large $\bar{a}$ corresponds to reduced opportunity for heat to spread, and, thus, a more one-dimensional flow of heat. The spreading resistance is also found to increase with increasing slab thickness. This may also be attributed to increased two-dimensionality of the temperature field for larger thickness slabs, where, the greater thickness facilitates greater spreading of heat. Note that Fig. 8 exhibits a saturation in terms of the impact of $\bar{t}$, in that while $\bar{t} = 0.1$ and $\bar{t} = 0.3$ curves are quite distinct, the curves at subsequently larger values of $\bar{t}$ are much closer to each other, implying that the thermal spreading resistance becomes increasingly insensitive to $\bar{t}$ for thick slabs.

The effect of $\bar{t}$ on spreading resistance can also be observed explicitly in Fig. 9, where the spreading resistance is plotted as a function of $\bar{t}$ for four different source half-widths. It is found, as expected that thermal spreading resistance increasing with $\bar{t}$, rapidly at first, and then saturating at larger values of $\bar{t}$. The thermal spreading resistance for small $\bar{t}$ is quite low, simply because a thin slab does not provide sufficient space for thermal spreading before the heat reaches the sink plane. On the other hand, the saturation at large $\bar{t}$ occurs mainly due to one-dimensional heat flow becoming increasingly dominant as the slab becomes thicker. Finally, as expected, Fig. 9 shows larger thermal spreading resistance at smaller $\bar{a}$, which is consistent with Fig. 8.

Finally, the impact of convective conditions at the sink plane is presented in Fig. 10, in which, the thermal spreading resistance is

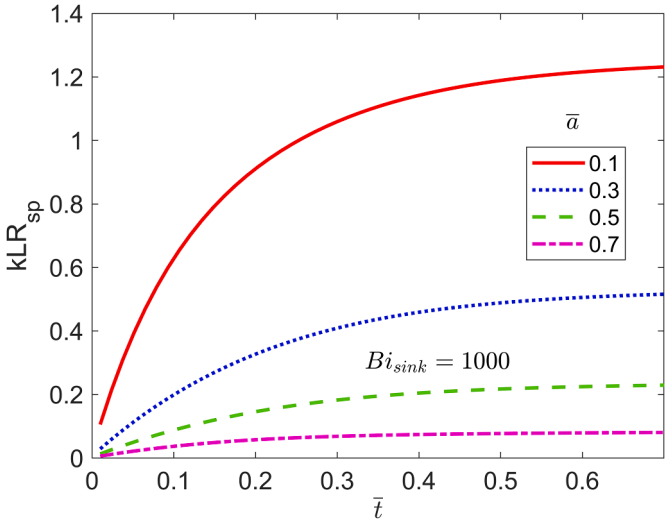

Fig. 9. Effect of slab thickness on thermal spreading resistance: Spreading resistance as a function of slab thickness $\bar{t}$ for multiple values of $\bar{a}$ with $Bi_{sink} = 1000$ for the slab problem.

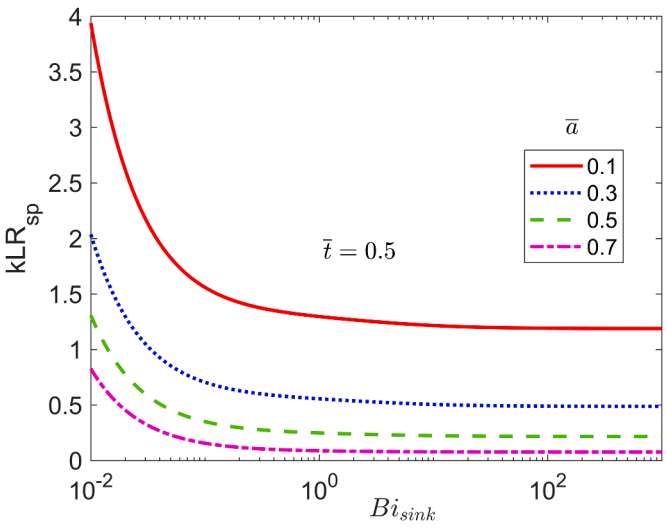

Fig. 10. Effect of sink plane convective condition on thermal spreading resistance: Spreading resistance as a function of sink Biot number Bi_{sink} for multiple values of $\bar{a}$ with $\bar{t} = 0.5$ for the slab problem.

plotted as a function of Bi_{sink}. The lower and upper ends in Bi_{sink} in Fig. 10 are representative of adiabatic and isothermal conditions, respectively. Fig. 10 shows that thermal spreading resistance reduces with increasing Bi_{sink}, including a strong saturation at large Bi_{sink} as conditions become more and more isothermal. Thermal spreading resistance is large at small Bi_{sink} because it suppresses thermal dissipation at the sink, resulting in reduced heat flow in steady state, and, therefore, greater thermal resistance. As Bi_{sink} increases, heat dissipation at the sink improves, allowing more flow of heat overall, and, therefore, reduced thermal spreading resistance. Finally, for sufficiently large values of Bi_{sink}, sink conditions are nearly isothermal, which is the best-possible heat dissipation scenario. As a result, further increase in Bi_{sink} does not appreciably reduce the thermal spreading resistance any more.

While Figs. 8–10 are presented for a finite-thickness slab, similar plots and parametric dependence is observed for the case of a finite-thickness cylinder as well.

5.7. Polynomial correlation for thermal spreading resistance

Thermal spreading resistance curves computed using the theoretical model presented here may be fitted with polynomial functions to result in approximate correlations that may be easier for an end-user for thermal design instead of the detailed calculations presented here. Since the thermal spreading resistance in this problem is a function of $\bar{a}$, $\bar{t}$ and Bi_{sink}, these correlations are developed for the spreading resistance as a function of $\bar{a}$, for multiple values of $\bar{t}$ and Bi_{sink}. In each case, the computed curve for spreading resistance as a function of $\bar{a}$ is fitted with the following correlation for the slab:

$$kLR_{sp} = c_0 + c_1\bar{a} + c_2\bar{a}^2 + c_3\bar{a}^3 \tag{28}$$

Values of c_0, c_1, c_2 and c_3 are reported in Table 1. Similar data for the cylindrical geometry are reported in Table 2. Except one case, the worst-case error over a range of $0.1 < \bar{a} < 0.5$ for slab and $0.2 < \bar{a} < 0.5$ for cylinder is found to be lower than 5% throughout. The error can be further reduced as desired by fitting with a higher-order polynomial.

Eq. (28) along with data in Tables 1 and 2 is expected to be a useful tool for a thermal designer without needing to enter into the mathematical details of the theoretical model presented here. For parameter values other than those listed in Tables 1 and 2, a MATLAB code for calculating the coefficients is available at https://github.com/jainautaedu/Rsp2023a (Slab) and https://github.com/jainautaedu/Rsp2023b (Cylinder). The code has been tested within the parameter

Table 1
Values of fitted correlation coefficients for thermal spreading resistance in a slab as a function of source half-width. Data are listed for different values of the slab thickness and sink Biot number.

(a) $Bi_{sink} = 1000$

	$\bar{t}$				
	0.1	**0.25**	**0.5**	**1.0**	**1.2**
c_0	1.094	1.642	1.886	1.978	1.994
c_1	-5.995	-7.926	-8.297	-8.458	-8.516
c_2	12.995	15.812	15.528	15.550	15.662
c_3	-10.023	-11.672	-11.142	-11.090	-11.175
Max. error (%)	6.29	3.44	2.48	2.29	2.28

(b) $Bi_{sink} = 10$

	$\bar{t}$				
	0.1	**0.25**	**0.5**	**1.0**	**1.2**
c_0	1.562	1.789	1.921	1.986	2.002
c_1	-7.861	-8.199	-8.337	-8.486	-8.545
c_2	16.116	15.780	15.458	15.604	15.720
c_3	-12.057	-11.452	-11.052	-11.131	-11.220
Max. error (%)	4.11	2.81	2.39	2.29	2.28

(c) $Bi_{sink} = 1.0$

	$\bar{t}$				
	0.1	**0.25**	**0.5**	**1.0**	**1.2**
c_0	2.945	2.202	2.049	2.054	2.068
c_1	-11.305	-8.737	-8.609	-8.749	-8.807
c_2	18.458	15.042	15.667	16.135	16.262
c_3	-12.098	-10.364	-11.138	-11.541	-11.641
Max. error (%)	1.27	1.81	2.19	2.25	2.24

(d) $Bi_{sink} = 0.1$

	$\bar{t}$				
	0.1	**0.25**	**0.5**	**1.0**	**1.2**
c_0	4.646	3.016	2.726	2.708	2.721
c_1	-13.751	-11.030	-11.191	-11.370	-11.429
c_2	16.666	18.793	20.950	21.590	21.721
c_3	-8.637	-13.202	-15.277	-15.787	-15.889
Max. error (%)	0.71	1.93	2.27	2.34	2.35

Table 2
Values of fitted correlation coefficients for thermal spreading resistance in a cylinder as a function of source radius. Data are listed for different values of the slab thickness and sink Biot number.

(a) $Bi_{sink} = 1000$

	$\bar{t}$				
	0.1	**0.25**	**0.5**	**1.0**	**1.2**
c_0	12.200	17.055	18.338	18.615	18.663
c_1	-67.814	-89.108	-92.110	-92.572	-92.713
c_2	137.325	173.352	174.801	174.774	175.001
c_3	-96.770	-119.250	-118.693	-118.409	-118.557
Max. error (%)	4.51	2.88	2.29	2.16	2.14

(b) $Bi_{sink} = 10$

	$\bar{t}$				
	0.1	**0.25**	**0.5**	**1.0**	**1.2**
c_0	16.635	17.949	18.454	18.639	18.687
c_1	-88.626	-91.598	-92.260	-92.642	-92.783
c_2	174.570	175.522	174.604	174.884	175.118
c_3	-120.938	-119.747	-118.409	-118.480	-118.634
Max. error (%)	3.28	2.50	2.24	2.15	2.13

(c) $Bi_{sink} = 1.0$

	$\bar{t}$				
	0.1	**0.25**	**0.5**	**1.0**	**1.2**
c_0	26.027	19.731	18.835	18.850	18.894
c_1	-121.818	-94.992	-92.997	-93.276	-93.416
c_2	218.897	175.364	174.975	175.945	176.192
c_3	-143.466	-117.334	-118.374	-119.186	-119.354
Max. error (%)	1.51	1.84	2.06	2.06	2.04

(d) $Bi_{sink} = 0.1$

	$\bar{t}$				
	0.1	**0.25**	**0.5**	**1.0**	**1.2**
c_0	32.698	22.334	20.964	20.920	20.963
c_1	-135.634	-101.359	-99.350	-99.607	-99.747
c_2	225.651	183.975	185.645	186.724	186.972
c_3	-141.535	-122.679	-125.550	-126.420	-126.589
Max. error (%)	0.86	1.26	1.48	1.50	1.49

range in Tables 1 and 2 and verified to produce results with lower than 5% error.

6. Conclusions

The key contribution of this work is in deriving a theoretical solution for the problem of thermal spreading resistance in a finite-thickness body with an isothermal source. In contrast, past work in this direction has mostly assumed an isoflux source. The limited available past work on an isothermal source is based on an approximate solution of the problem using a flux distribution that produces a nearly, but not exactly, isothermal source. Moreover, past work is also often limited in other ways, such as requiring a small source, and, in the case of available results for a cylinder, an isothermal sink instead of more general convective conditions. Comparison of the present results with such past work shows similar trends, with greater accuracy expected from the present results.

Expressions for the non-dimensional thermal spreading resistance for slab and cylinder geometries may be helpful for design and optimization of thermal systems in which thermal spreading or constriction play an important role. The third-order polynomial fits of key results may be of particular interest to end-use designers, as these correlations may facilitate thermal design without the need for detailed mathematical calculations and with reasonable accuracy.

CRediT authorship contribution statement

Ankur Jain: Conceptualization, Methodology, Formal analysis, Validation, Investigation, Data curation, Project administration, Writing – original draft, Writing – review & editing.

Declaration of Competing Interest

The authors declare that they have no known competing financial

interests or personal relationships that could have appeared to influence the work reported in this paper.

Data availability

Data will be made available on request.

Acknowledgments

The author would like to acknowledge an excellent webinar presentation by Prof. Marc Hodes and Prof. Yuri S. Muzychka that introduced him to the topic of thermal spreading resistance.

References

[1] M.M. Yovanovich, Conduction and thermal contact resistances (conductances), in: W.M. Rohsenow, J.P. Hartnett, Y.I. Cho (Eds.), Handbook of Heat Transfer, 3rd Ed., McGraw-Hill, 1998.
[2] M.M. Yovanovich, E.E. Marotta, Thermal spreading and contact resistances, in: A. Bejan, A. Kraus (Eds.), Heat Transfer Handbook, John Wiley & Sons, 2003.
[3] S. Lee, S. Song, V. Au, K.P. Moran, Constriction/spreading resistance model for electronics packaging, in: Proc. ASME/JSME Thermal Engineering Conference 4, 1995, pp. 199–206.
[4] M.M. Yovanovich, C.L. Tien, G.E. Schneider, General solution of constriction resistance within a compound disk, Heat Transf. Thermal Control Heat Pipes 70 (1980) 47–62, https://doi.org/10.2514/5.9781600865442.0047.0062. AIAA.
[5] K.S. Ong, C.F. Tan, K.C. Lai, K.H. Tan, Heat spreading and heat transfer coefficient with fin heat sink, Appl. Thermal Eng. 112 (2017) 1638–1647, https://doi.org/10.1016/j.applthermaleng.2016.09.161.
[6] S. Lee, M.M. Yovanovich, S. Song, K.P. Moran, Analysis of thermal constriction resistance in bolted joint,', Int. J. Microcircuits Electron. Packag. 16 (1993) 125–136.
[7] I. Hirsch, E. Berman, N. Haik, Thermal resistance evaluation in 3-D thermal simulation of MOSFET transistors, Solid-State Electron. 36 (1993) 106–108, https://doi.org/10.1016/0038-1101(93)90076-3.
[8] I. Sauciuc, G. Chrysler, R. Mahajan, R. Prasher, Spreading in the heat sink base: phase change systems or solid metals, IEEE Trans. Components Packag. Technol. 25 (2002) 621–628, https://doi.org/10.1109/TCAPT.2002.807994.
[9] Y.C. Hua, H.L. Li, B.Y. Cao, Thermal spreading resistance in ballistic-diffusive regime for GaN HEMTs, IEEE Trans. Electron. Dev. 66 (2019) 3296–3301, https://doi.org/10.1109/TED.2019.2922221.
[10] K.S. Yang, C.H. Chung, C.W. Tu, C.C. Wong, T.Y. Yang, M.T. Lee, Thermal spreading resistance characteristics of a high power light emitting diode module, Appl. Thermal. Eng. 70 (2014) 361–368, https://doi.org/10.1016/j.applthermaleng.2014.05.028.
[11] S. Karmalkar, P.V. Mohan, H.P. Nair, R. Yeluri, Compact models of spreading resistances for electrical/thermal design of devices and ICs, IEEE Trans. Electron. Dev. 54 (2007) 1734–1743, https://doi.org/10.1109/TED.2007.899371.
[12] L.E. Dickens, Spreading resistance as a function of frequency, IEEE Trans. Microwave Theory Tech. 15 (1967) 101–109, https://doi.org/10.1109/TMTT.1967.1126383.
[13] L. Zhang, E.P. Li, X.P. Yu, R. Hao, Modeling and optimization of substrate electromagnetic coupling and isolation in modern lightly doped CMOS substrate, IEEE Trans. Electromag. Compat. 59 (2017) 662–669, https://doi.org/10.1109/TEMC.2016.2629702.
[14] D.P. Kennedy, Spreading resistance in cylindrical semiconductor devices, J. Appl. Phys. 31 (1960) 1490–1497, https://doi.org/10.1063/1.1735869.
[15] B.B. Mikic, W.M. Rohsenow, Thermal contact resistance, Mech. Eng. Rep. (1966). DSR 74542-41.
[16] Y.S. Muzychka, M.M. Yovanovich, J.R. Culham, Thermal spreading resistance in compound and orthotropic systems, J. Thermophys. Heat Transf. 18 (2004) 45–51, https://doi.org/10.2514/1.1267.
[17] M.M. Yovanovich, V.W. Antonetti, Application of thermal contact resistance theory to electronic packages, in: A. Bar-Cohen, A.D. Kraus (Eds.), Advances in Thermal Modeling of Electronic Components and Systems, Hemisphere Publishing, New York, 1988.
[18] H.S. Carslaw, J.C. Jaeger, Conduction of Heat in Solids, Clarendon Press, Oxford, 1959.
[19] Y.S. Muzychka, M.M. Yovanovich, J.R. Culham, Influence of geometry and edge cooling on thermal spreading resistance, J. Thermophys. Heat Transf. 20 (2004) 247–255, https://doi.org/10.2514/1.14807.
[20] Y.S. Muzychka, M.R. Sridhar, M.M. Yovanovich, V.W. Antonetti, Thermal spreading resistance in multilayered contacts: applications in thermal contact resistance, J. Thermophys. Heat Transf. 13 (1996) 1–11, https://doi.org/10.2514/6.1996-3967.
[21] R.U. Sexl, D.G. Burkhard, An exact solution for thermal conduction through a two-dimensional eccentric constriction, Prog. Astronaut. Aeronaut. 21 (1969) 617–620, https://doi.org/10.2514/5.9781600864957.0617.0620.
[22] Y.S. Muzychka, K.R. Bagnall, E.N. Wang, Thermal spreading resistance and heat source temperature in compound orthotropic systems with interfacial resistance, IEEE Trans. Components Packag. Manuf. Technol. 3 (2013) 1826–1841, https://doi.org/10.1109/TCPMT.2013.2269273.
[23] M.G. Cooper, B.B. Mikic, M.M. Yovanovich, Thermal contact conductance, Int. J. Heat Mass Transf. 12 (1969) 279–300, https://doi.org/10.1016/0017-9310(69)90011-8.
[24] Veziroglu, T.N., Chandra, S. 'Thermal conductance of two-dimensional constrictions,' Paper 68–791, AIAA 3rd Thermophysics Conf., Los Angeles, CA. DOI: 10.2514/5.9781600864957.0591.0615.
[25] G. Gladwell, T. Lemczyk, Thermal constriction resistance of a contact on a circular cylinder with mixed convective boundaries, Proc. R. Soc. A 420 (1988) 323–354, https://doi.org/10.1098/rspa.1988.0129.
[26] I. Sneddon, Mixed Boundary Value Problems in Potential Theory, North-Holland Publishing Company, 1966.
[27] A. Hunter, A. Williams, Heat flow across metallic joints—the constriction alleviation factor, Int. J. Heat Mass Transf. 12 (1969) 524–526, https://doi.org/10.1016/0017-9310(69)90148-3.
[28] Hahn, D.W., Özışık, M.N., 'Heat Conduction,' 3rd ed., Hoboken, N.J., Wiley, 2012. ISBN: 978-0-470-90293-6.
[29] G. Krishnan, A. Jain, Theoretical analysis of a two-dimensional multilayer diffusion problem with general convective boundary conditions normal to the layered direction, Int. J. Heat Mass Transf. 202 (2023), 123723, https://doi.org/10.1016/j.ijheatmasstransfer.2022.123723.
[30] D. Sarkar, K. Shah, A. Haji-Sheikh, A. Jain, Analytical modeling of temperature distribution in an anisotropic cylinder with circumferentially-varying convective heat transfer, Int. J. Heat Mass Transf. 79 (2014) 1027–1033, https://doi.org/10.1016/j.ijheatmasstransfer.2014.08.060.
[31] S.W. Ma, A.I. Behbahani, Y.G. Tsuei, Two-dimensional rectangular fin with variable heat transfer coefficient, Int. J. Heat Mass Transf. 34 (1991) 79–85, https://doi.org/10.1016/0017-9310(91)90175-E.
[32] M. Abramowitz, I.A. Stegun, Handbook of Mathematical Functions, Dover, New York, 1965.